GSA Data Repository 2018072

Mungall et al., 2018, Immiscible shoshonitic and Fe-P-oxide melts preserved in unconsolidated tephra at El Laco volcano, Chile: Geology, https://doi.org/10.1130/G39707.1.

Compositional data are presented in Excel file Table DR1, DR2, DR3.

Methods:

Polished thick sections of the sample of the friable El Laco magnetite bomb were made by impregnating the sample with epoxy and cutting the section in the absence of water to ensure that no loss of a water-soluble iron phosphate species occurred. Thick sections of the EL96-3 volcanic ash sample were also mounted and polished in the absence of water.

The magnetite bomb thick sections were then imaged for composition using Backscattered Electron (BSE) imaging on a JEOL JSM840 scanning electron microscope (SEM) using a 15 kV or 20 kV accelerating voltage.

The composition of the glass phases from the hematite bomb and the experiments was determined quantitatively using an Electron Probe X-Ray Microanalyzer with a 15.0 kV accelerating voltage and a 10.0 nanoamp beam current with a beam size of 10 microns. The standard for Si, Al, Fe, Mg, and Ca was basaltic glass 'basaltsx1'. Standards were rutile (Ti), bustamite (Mn), pentlandite (S), sanidine (K), apatite (P), Cr2O3 (Cr), phlogopite (F), and tugtupite (Cl). X-rays were counted for equal times on peak and on background on either of the peaks. Fe-P-O glasses were analyzed in a similar manner but the standards used were hematite (Fe), V2O5 (V), apatite (Ca, P), rutile (Ti), Cr2O3 (Cr), biotite (Al), bustamite (Mn), chalcopyrite (S), tugtupite (Cl), albite (Na), sanidine (K). The results obtained for the composition of the silicate and phosphate glasses are shown in Table DR1 and DR2, respectively.

A whole rock analysis was performed on the EL96-3 sample of a volcanic ash of hematite minor magnetite and minor iron phosphate using a Phillips PW2405 x-ray flourescence spectrometer. The ash sample was first ground down to a fine powder under ethanol and then analyzed as a pressed powder sample. The semi-quantitative results are shown in Table DR3.

The powdered EL96-3 volcanic ash sample was then analyzed using x-ray diffraction to determine the species of iron phosphate present in the ash. For this analysis a Philips PW 3710 mpd control with a PW 1830 generator, a PANalytical Long Fine Focus Cu tube, and a Philips PW 3011 detector was used.

A portion of the sample of EL96-3 hematite volcanic ash was prepared for a 1 atm melting experiment. The sample was ground down to a fine powder under ethanol and dehydrated in a furnace at 800°C over 15 hours. The heating of the sample could have oxidized any remaining magnetite in the sample to hematite. Before dehydration, the weight of the sample was 2.5691g. After dehydration the sample weight was found to be 2.5566g. A hematite-magnetite buffer was prepared using 101.1mg of Fe(III) and 101.1mg of Fe(II and III). The mixture was ground to a fine powder under ethanol using an agate mortar and pestle. After the ethanol had evaporated, the buffer was loaded into a 7mm outer diameter, 5mm inner diameter silica glass tube. A silica glass capsule just large enough to fit into the silica glass tube was then packed with 155.7mg of the dehydrated and potentially oxidized hematite volcanic ash and minor iron phosphate sample and inserted into the silica glass tube on top of the magnetite hematite buffer. A silica glass spacer was then inserted into the tube on top of the silica glass capsule and magnetite

hematite buffer. The silica tube was then evacuated under vacuum for 30 minutes and sealed just above the silica glass spacer. The tube was put into a furnace at 1081°C and 1 atmosphere for 6 hours and then quenched in a beaker of 25°C water. After the experiment the sample was found to be slightly magnetic and the buffer was very magnetic. The sample was cut out of the tube in the presence of water, mounted in epoxy and polished to 1 micron.

The buffer was then analyzed after the experiment using x-ray diffraction to determine the species of iron oxide remaining in the buffer. For this analysis a Philips PW 3710 mpd control with a PW 1830 generator, a PANalytical Long Fine Focus Cu tube, and a Philips PW 3011 detector was used. Both magnetite and hematite remained in the buffer.

The epoxy mounted sample was then carbon coated and imaged for composition using Backscattered Electron (BSE) imaging on a JEOL JSM6610-Lv SEM using a 15kV accelerating voltage. Semi-quantitative compositional analysis was performed using an Oxford/SDD EDS detector (ultra thin window) to obtain a rough composition of the glass phase in the sample. The semi-quantitative compositions of the glass phase and remaining crystalline phases in the sample are shown in Table DR3.

Piston cylinder experiments were conducted in a 3/4" end-loaded device at the University of Toronto using a crushable ceramic inner assembly enclosed in cylindrical graphite furnace, pyrex sleeve, and a NaCl pressure medium. Pressure was measured by a Bourdon gauge and has not been corrected for friction. Temperature was monitored by a Type S thermocouple. Runs were quenched by turning off power to the heater.

Chemography.

The behavior of the system Fe-C-O was investigated by Weidner (1982) using reduced starting materials. The bulk compositions of the charges were all within the field between siderite, graphite, hematite and wüstite, produced as various mixtures of siderite, graphite, hematite, and iron. None of Weidner's starting compositions were sufficiently oxidized to fall within the field of CO_2-magnetite-hematite, which might better approximate natural iron formations or their putative melting products. We therefore have addressed the possible topologies of the phase diagram at higher fO_2, where experimental data are absent but basic principles of chemography permit the possible topologies to be explored as a basis for qualitative interpretation of natural assemblages. Because the compositions of the liquids and vapors are unconstrained, we must at times consider multiple topologies for the reactions.

Henceforth we refer to phases by the following abbreviations: I = iron; W = wüstite; G = graphite; V = C-O vapor of uncertain composition; M = magnetite; H = hematite; L = Fe-O-C liquid of uncertain composition. We assume that the reader is familiar with Weidner's work in all its details.

Figure DR1 shows the system Fe-O-C and the locations of the principal phases that might exist in the system. The plausible range of compositions of a C-bearing Fe oxide melt is shown by a dashed line labeled 'liquid'. The plausible range of compositions of C-O vapors stretching between CO and CO_2 is shown as another dashed line labeled 'vapor'. Figure DR2 shows possible arrangements of phase compositions and tie-lines for each of three invariant points I_1 through I_3. Due to the range of possible compositions of the liquid phase, there are three plausible topologies for each of I_1 (W+M+G+L+V) and I_2 (I+W+G+L+V). The first two invariant points were presented by Weidner (1982) in his Figures 2 and 3, which are reproduced here as Figures DR3 and DR4; evidently his experimental results define the actual

reactions that occur at these low fO2s and thereby constrain the approximate composition of the liquid. The experimental constraints allow a choice between the competing possible topologies corresponding to the inset chemographic diagram in the upper left of each of Figures DR3 and DR4.

A third invariant point I_3, H+M+G+L+V, must exist in systems at higher fO_2 where hematite is a stable phase (c.f., Weidner's 1982 Figure 5). Invariant point I_3 must be joined to I_2 along the wüstite-absent reaction emanating from I_2, since by definition I_3 does not contain wüstite. Hence I_3 can be placed in its correct approximate position in Figure DR5 even though we do not know the exact P, T at which it exists. Due to our uncertainty about the composition of the liquid, which must become more oxygen-rich as fO_2 increases between I_2 and I_3, we again show three possible topologies in Figure DR4, one of which is expressed in detail in Figure DR5. The insets in Figure DR5 show the phase assemblage in each field bounded by the reaction curves for the topology defined by the inset in the top left, which was identified in Figure DR4 as the "I_3 to match Weidner"; i.e., the liquid composition selected for this possibility remains in the same compositional field as that required to satisfy the topology observed around I_2 by Weidner (1982). The reactions in Figure DR5 are redrawn in Figure DR6 with the reactants and products on the correct sides of the boundaries to aid in interpretation.

The key decompression reaction in Figures DR5 and DR6 is the graphite-absent reaction labeled [G] in Figure DR5 and H+L = M+V in Figure DR6. At somewhat more oxygenated conditions, the reactions entitled "I_3 at higher temperature, higher fO_2" in the top right of Figure DR2 will apply; however the key decompression reaction H+L = M+V remains unchanged.

If, however, the liquid is much more oxygen-rich at high fO_2 than it is at I_2, falling in the M-H-V field, then the decompression reaction becomes L = M+H+V.

Regardless of the oxygen content of the Fe-O-C liquid in the vicinity of invariant point I_3, decompression of the liquid will cause solidification of magnetite and or hematite along with the spontaneous evolution of large volumes of C-O vapor. We conclude from this qualitative exercise in chemography that decompression of Fe oxide liquid fluxed by carbonic fluid will cause rapid compositional undercooling and crystallization of iron oxides simultaneous with potentially highly explosive gas emissions.

Figure DR1

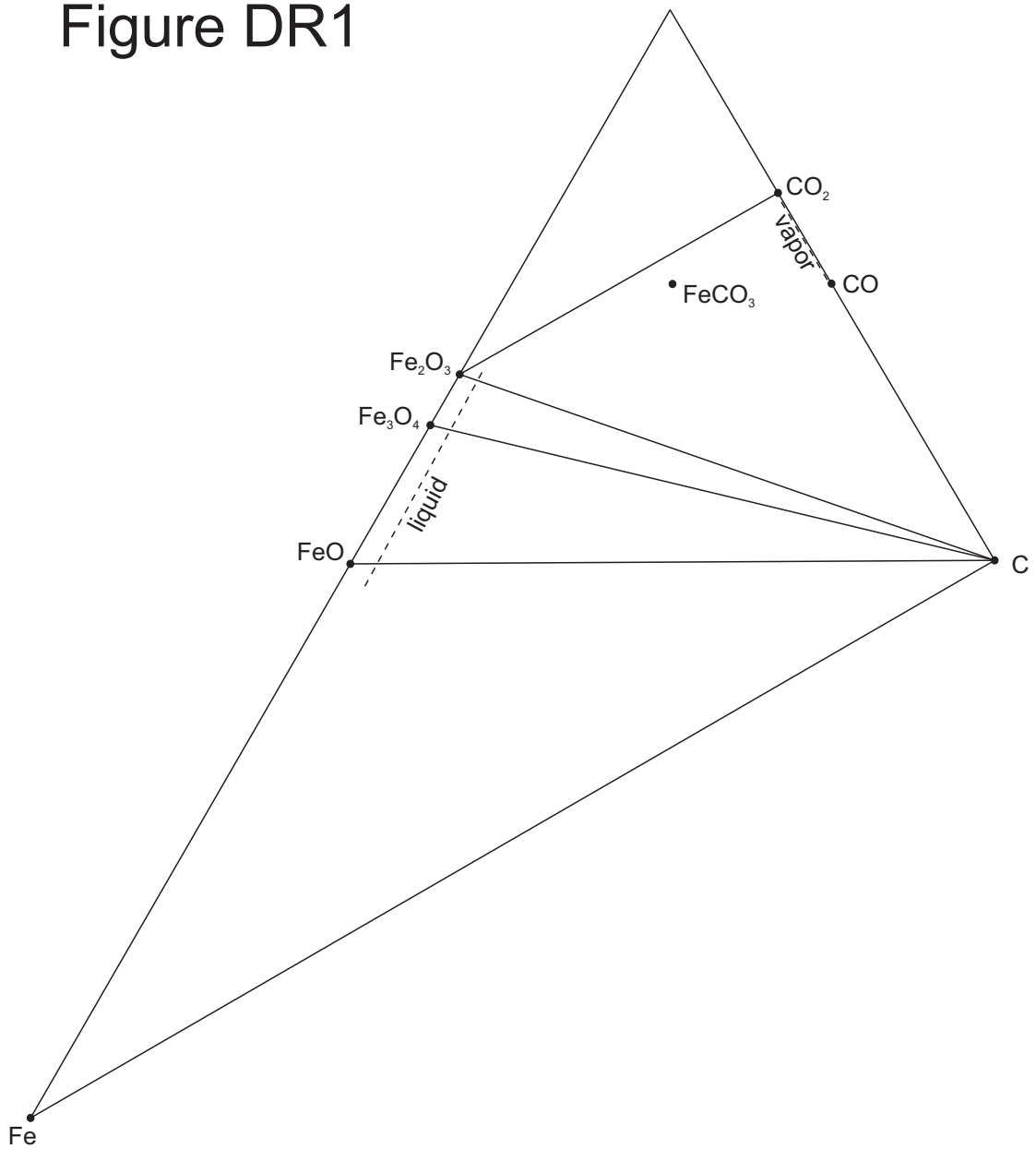

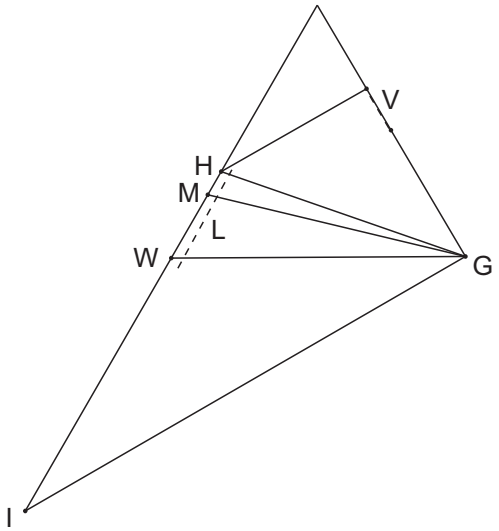

I_3 at highest temperature, highest fO_2

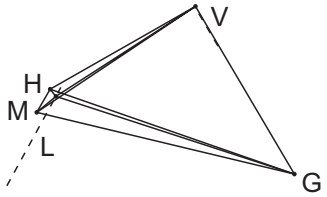

H+G=L+V [M]
H+M+G=L [V]
M+V=L+G [H]
H+M+V=L [G]
M+V=H+G [L]

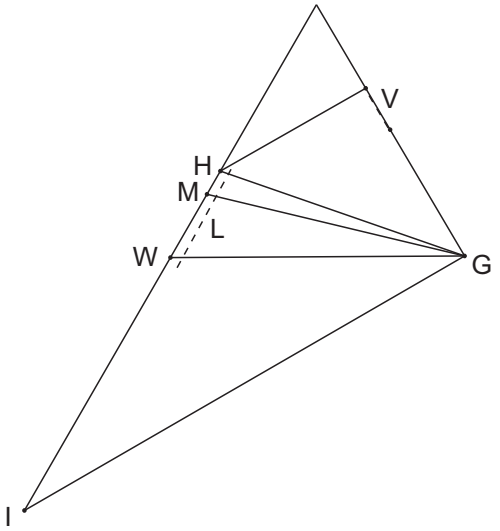

I_1 at lowest temperature, lowest fO_2

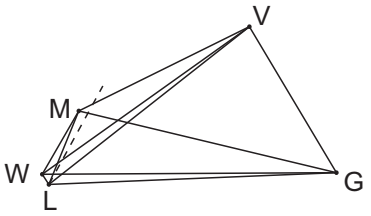

L+V=W+G [M]
L+M=W+G [V]
M+G=L+V [W]
W+V=L+M [G]
W+V=M+G [L]

I_2 at lowest temperature, lowest fO_2

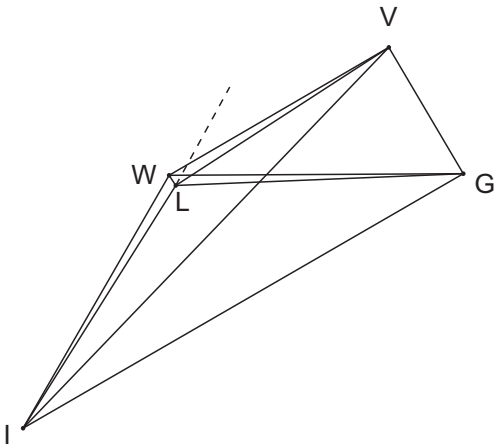

W+G=L+V [I]
I+W+G=L [V]
I+V=L+G [W]
I+W+V=L [G]
W+G=I+V [L]

I_3 at higher temperature, higher fO_2

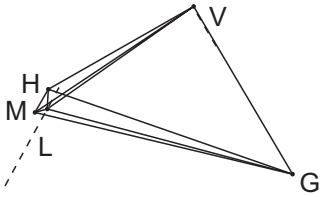

H+G=L+V [M]
H+M+G=L [V]
M+G+V=L [H]
M+V=H+L [G]
M+V=H+G [L]

I_3 to match Weidner (1982)

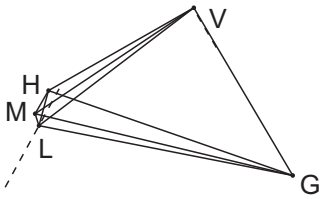

H+G=L+V [M]
M+G=H+L [V]
M+G=L+V [H]
M+V=H+L [G]
M+V=H+G [L]

I_1 at higher temperature, higher fO_2

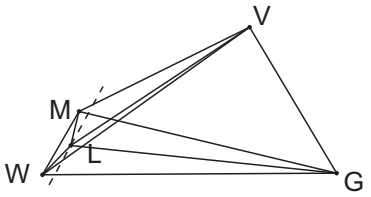

L+G=W+V [M]
L=W+M+G [V]
M+G=L+V [W]
L=W+M+V [G]
W+V=M+G [L]

I_1 in Weidner (1982)

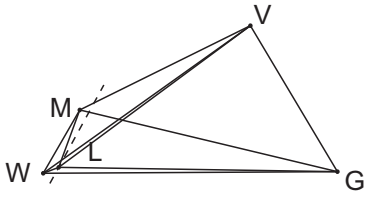

L=W+G+V [M]
L=W+M+G [V]
M+G=L+V [W]
W+V=L+M [G]
W+V=M+G [L]

I_2 at higher temperature, higher fO_2

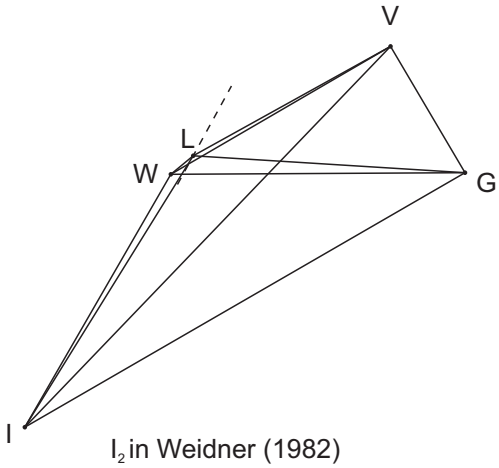

L+G=W+V [I]
L+I=W+G [V]
I+V=L+G [W]
W+V=L+I [G]
W+G=I+V [L]

I_2 in Weidner (1982)

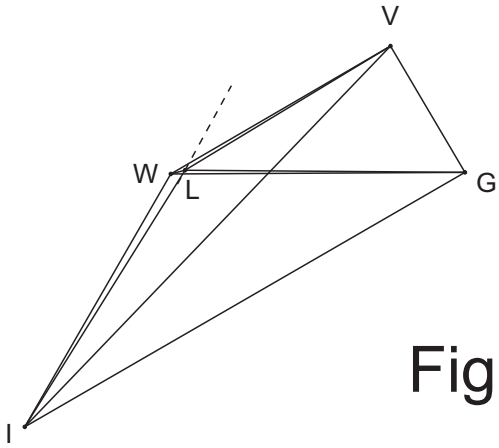

W+G+V=L [I]
W+G=I+L [V]
I+V=L+G [W]
I+W+V=L [G]
W+G=I+V [L]

Figure DR2

Figure DR3

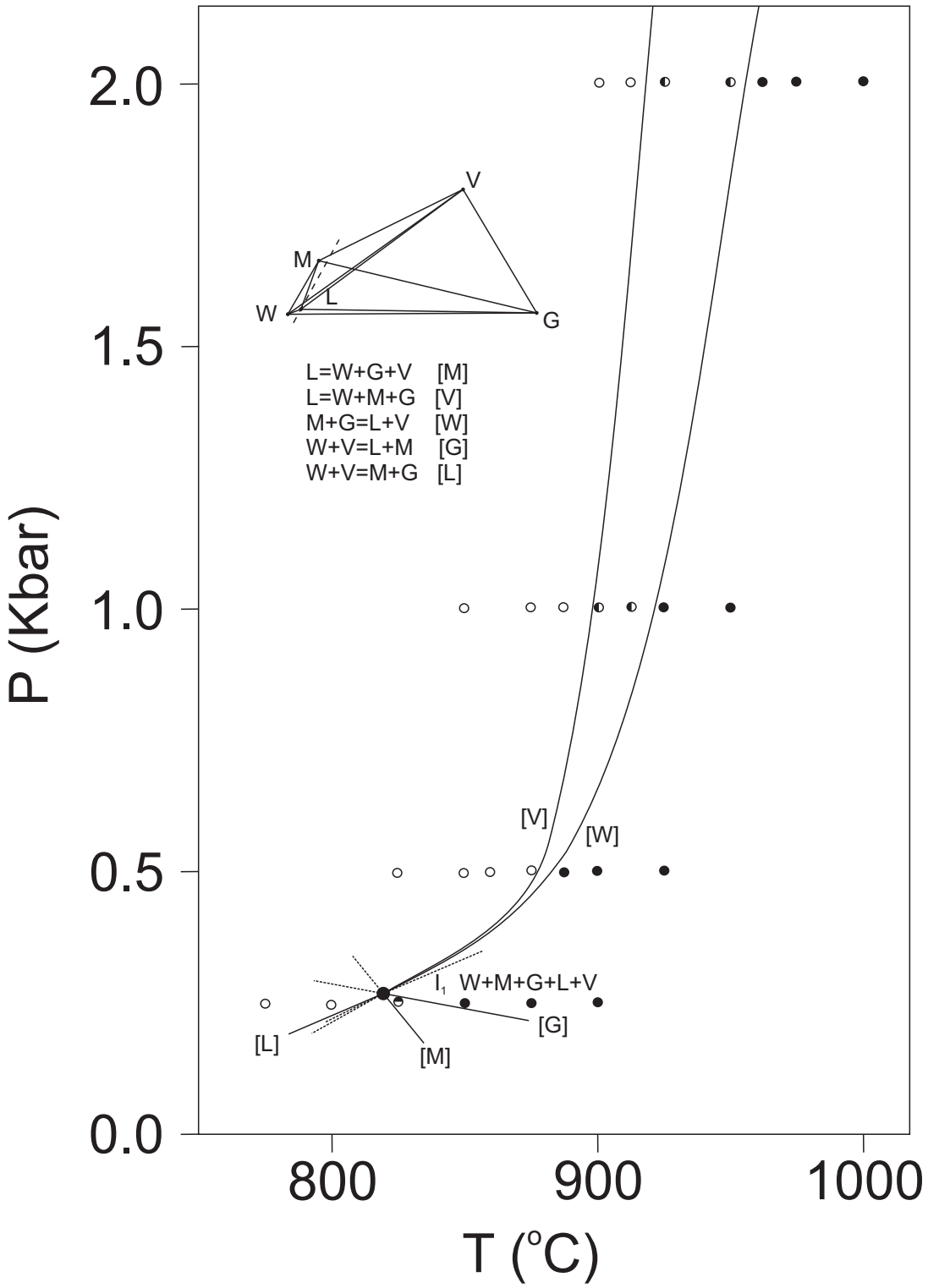
2.0
1.5
1.0
0.5
0.0
P (Kbar)
800
900
1000
T (°C)
V
M
L
W
G
L=W+G+V [M]
L=W+M+G [V]
M+G=L+V [W]
W+V=L+M [G]
W+V=M+G [L]
[V]
[W]
I1 W+M+G+L+V
[G]
[L]
[M]

Figure DR4

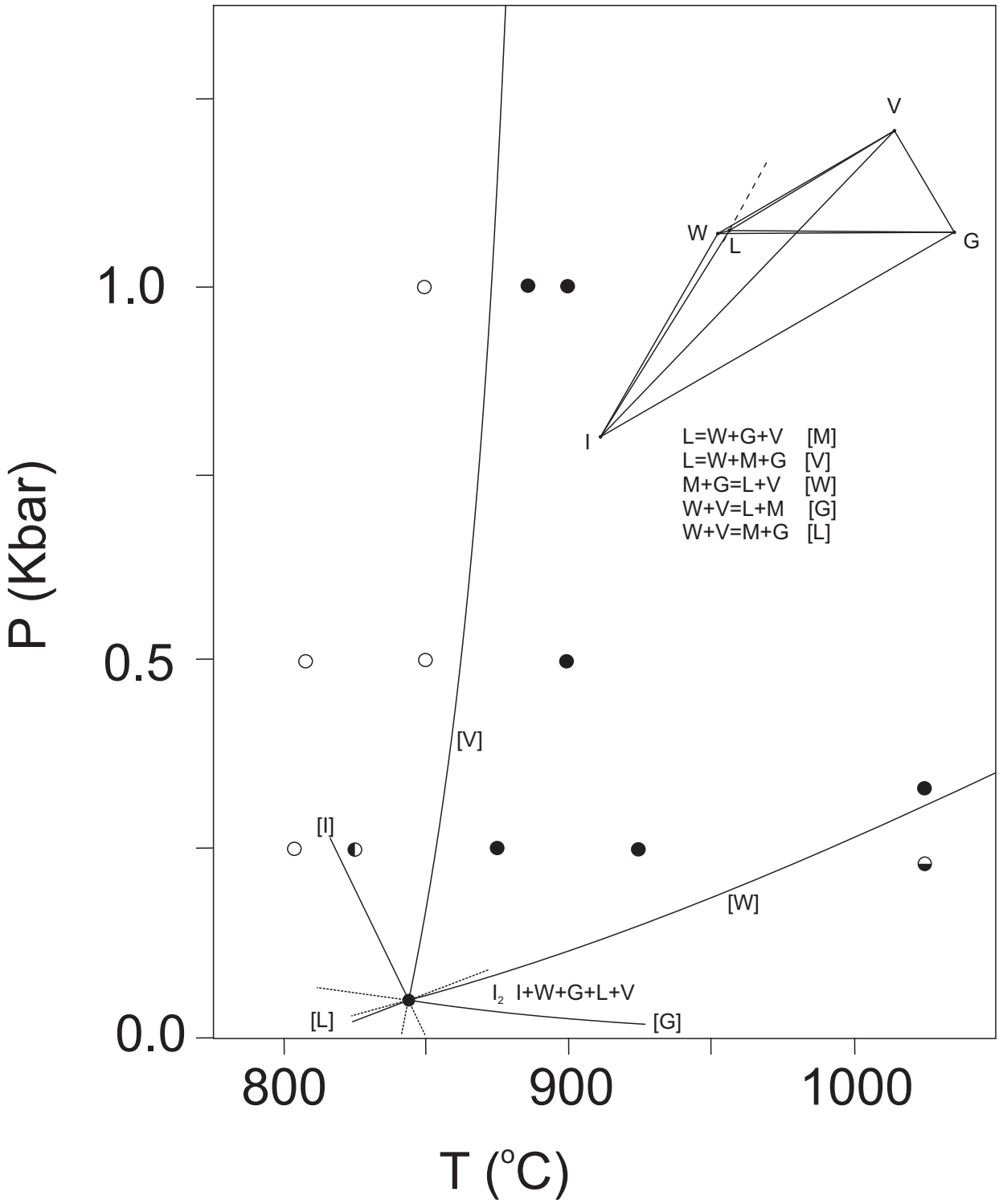
V
W
L
G
I
L=W+G+V [M]
L=W+M+G [V]
M+G=L+V [W]
W+V=L+M [G]
W+V=M+G [L]
1.0
0.5
0.0
P (Kbar)
[V]
[I]
[W]
[L]
[G]
I_2 I+W+G+L+V
800
900
1000
T (°C)

Figure DR5

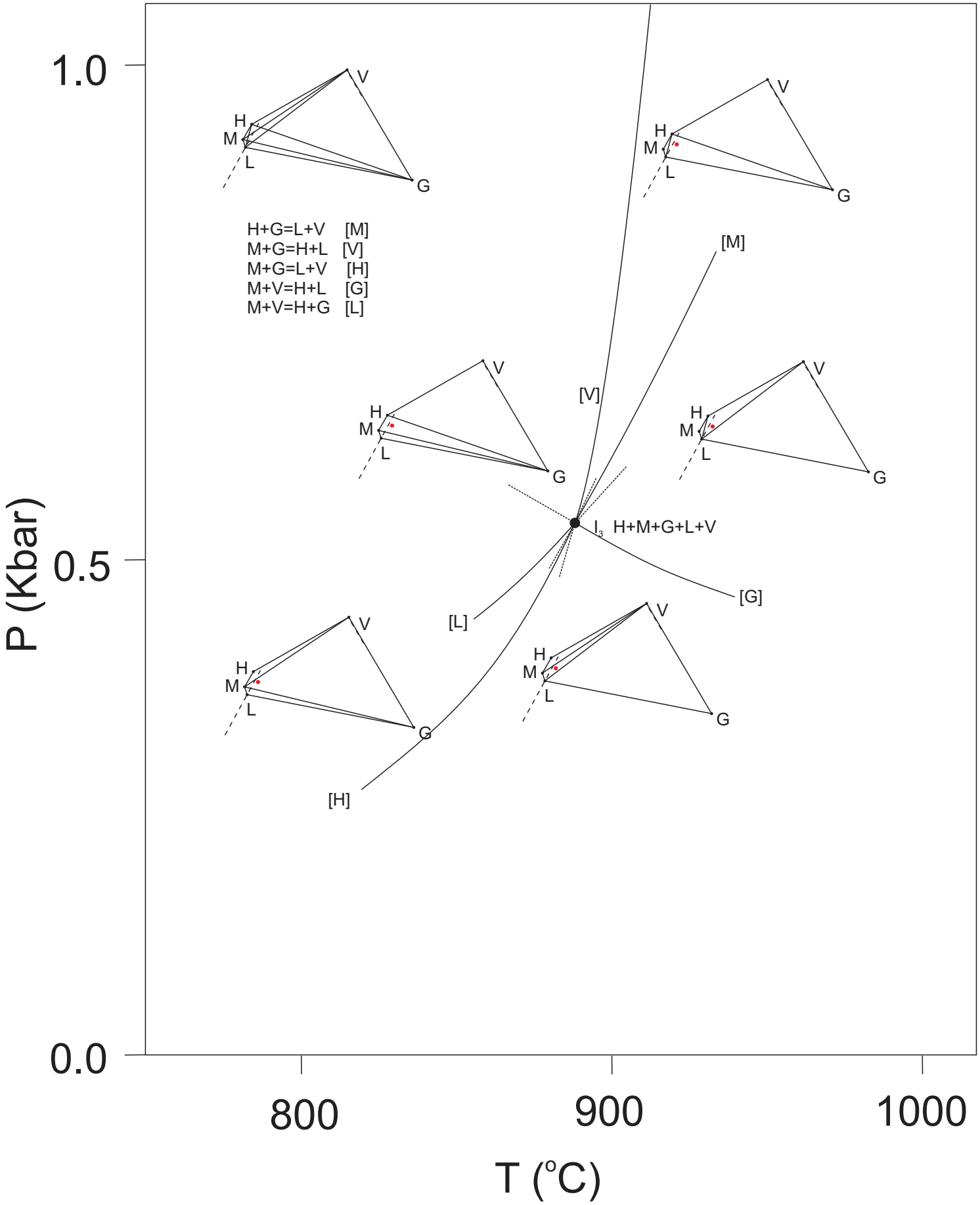
1.0
0.5
0.0
P (Kbar)
800
900
1000
T (°C)
H+G=L+V [M]
M+G=H+L [V]
M+G=L+V [H]
M+V=H+L [G]
M+V=H+G [L]
[M]
[V]
[G]
[L]
[H]
I3 H+M+G+L+V
V
H
M
L
G

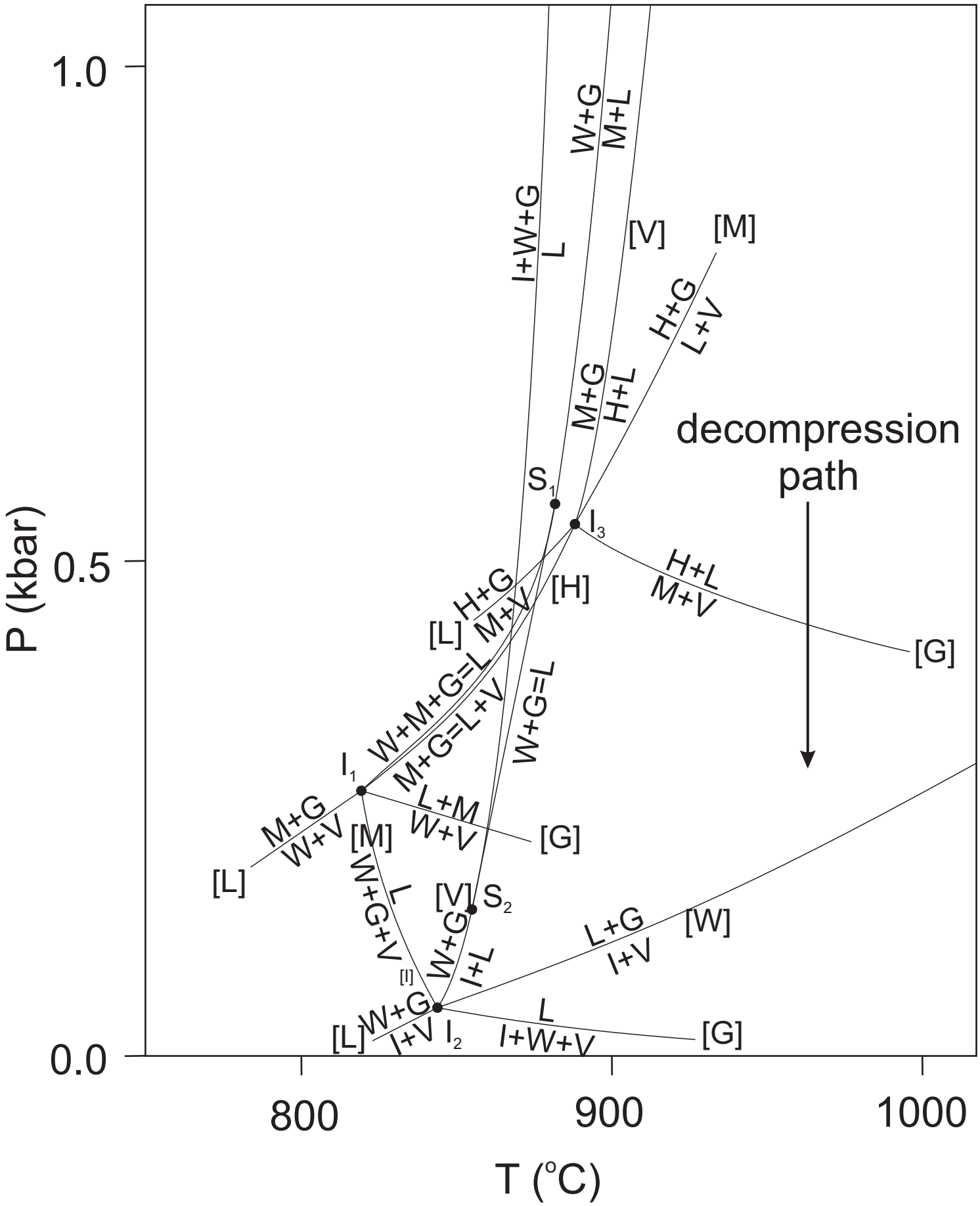
1.0
0.5
0.0
P (kbar)
800
900
1000
T (°C)
I+W+G
L
W+G
M+L
[V]
[M]
H+G
L+V
M+G
H+L
decompression
path
S1
I3
H+L
M+V
[G]
H+G
M+V
[H]
[L]
W+M+G=L
W+G=L
M+G=L+V
I1
L+M
W+V
[G]
M+G
W+V
[M]
[L]
W+G+V
L
[V]
S2
W+G
I+L
[I]
L+G
I+V
[W]
W+G
I+V
I2
L
I+W+V
[G]
[L]